

CHEMISTRY & BIOLOGY INTERFACE

An official Journal of ISCB, Journal homepage; www.cbijournal.com

In Vitro biological evaluations of copper complexes: Phenyl-quinoline derivatives of novel organoselenium compounds as therapeutic agent.

P. Moohambihai ^a, K. Nagashri ^b

^aResearch scholar (Registration Number : 18224012032016), Department of Chemistry, Manonmaniam Sundaranar University, Tirunelveli-627012, Tamilnadu, India.

^bDepartment of Chemistry, Manonmaniam Sundaranar University, Tirunelveli-627012, Tamilnadu, India.

Email address: ambikachem12@gmail.com, shrik1810@gmail.com

Received; 8 Feb 2022, Accepted; 28 February 2022

Abstract: Copper (II) complexes (3a-i) with (16E)-N-(2-phenylquinolin-4(1H)-ylidene)-2-(phenylselanyl) benzenamine ligands were synthesized. They were characterized by various spectroscopic studies. In-vitro cytotoxic potential was determined, with significant cytotoxicity against MCF-7 cell line. The copper complexes interacted with the calf thymus - DNA, (CT-DNA), according to absorption spectra and viscosity measurements. In addition, the copper complexes were tested for antimicrobial activity against three Gram-negative bacteria; *Proteus vulgaris*, *Klebsiella pneumoniae*, and *Shigella flexneri*, three Gram-positive bacteria; *Staphylococcus aureus*, *Staphylococcus epidermidis*, and *Bacillus subtilis*, and three fungi; *Aspergillus fumigatus*, *Aspergillus clavatus* and *Candida albicans*. The ligand's acetylcholinesterase (AChE) inhibiting function was investigated in order to determine the ligand's efficacy in the treatment of neurodegenerative disorders. When compared to standard Rivastigmine and Galantamine, the synthesized ligand 2c showed selective inhibition (AChE & BuChE) with IC₅₀ values of 0.20 and 3.03 μM. The egg albumin method was used to test the anti-inflammatory efficiency and α-glucosidase inhibitory activities of copper chelates were tested.

Key-words: Antimicrobial, Cytotoxicity, DNA binding, α-glucosidase and Phenylselanyl-quinoline.

1.0 Introduction

Schiff bases are a class of compounds that can chelate, redox active transition metal ions via the -CH=N or Ar-O- atoms. They have a wide range of uses in pharmaceutical [1, 2], catalyst [3-5], polymer synthesis, energy sensors,

industrial chemistry [6], and other fields. Copper, cobalt, nickel, and zinc complexes are more promising among transition metals due to their redox behaviour, low toxicity, and presence in biological molecules [7].

Chemical structural modifications of known

therapeutic molecules are an important approach to the drug development process. Heterocyclic moieties, which are found in a variety of compounds, play an important role in a variety of biological processes [8].

The biological activity of these compounds is primarily determined by their molecular structures. A nitrogen-containing scaffold, quinoline core is a potent pharmacophoric moiety in existing drug molecules [9–11].

When selenium combines with quinoline, it becomes active in the research area. The selenium atom is also known to play a key role in the mode of action of certain proteins, which cannot be done by its closest relative, sulphur [12]. Synthetic organoselenium compounds have also been found to act as anti-oxidants, chemopreventers, and apoptosis inducers in a variety of organs, including brain, liver, skin, colon, lung, and prostate [13, 14].

Selenium atom is a valuable methodology for constructing a variety of five- and six-membered selenium-containing heterocyclic compounds that requires more attention. Alzheimer's disease is a progressive illness that describes a decline in cognitive capacity, memory loss, and other mental issues. In the present situation, it is the sixth most lethal disease in the world, affecting nearly 50 million people. Changes in the activities of acetyl cholinesterase (AChE) and butyl cholinesterase (BuChE) were observed in the cerebral cortex and hippocampus and were linked to disease progression. Many AChE inhibitors have been studied, and researchers are still working to develop some new pharmacologically profiled drug molecules [15, 16].

Because of the neurotransmitter acetylcholine deficiency in the brain, AChE and BuChE levels are vary irregularly in Alzheimer's disease. With a better understanding of the

relationship between AChE and BuChE levels, Alzheimer's disease can be easily tracked and managed. The majority of drugs available on the market for potential treatment of AD are cholinesterase inhibitors (Galantamine, Donepezil, Rivastigmine).

Inhibitors of cholinesterase that block both AChE and BuChE, as well as highly selective BuChE inhibitors, could be useful in treating Alzheimer's disease and other dementias. Both enzymes are still important targets in therapeutic development for Alzheimer's disease. The difficult task is always to synthesise a redox active and conjugated planar molecule with increased bioactivities against a specific target. This study concentrated on novel cholinesterase inhibitors as potential anti-multifunctional Alzheimer's agents.

The synthesis and spectroscopic elucidation of copper chelates were performed and presented in this study. Various spectroscopic techniques were used to characterise the prepared complexes. The antimicrobial, cytotoxicity, anti-inflammatory, DNA binding and α -Glucosidase inhibitory activities of phenylselenylquinoline derivatives and their chelates were investigated.

2.0 Experimental

In this experiment, AnalaR grade chemicals were used. To record the NMR spectra of the ligands, tetramethylsilane (TMS) was used as an internal standard. In comparison to TMS, chemical changes (δ) are measured in parts per million. The ligands and their complexes' Fast Atom Bombardment mass spectra (FAB) were recorded on a Jeol SX 102/DA-6000 mass spectrometer/data system with argon/xenon (6 kV, 10 mA) as the FAB gas. The molar conductance of copper complexes in DMSO solution was measured using a coronation digital conductivity meter. The IR spectra of the ligands and their copper complexes were measured in

the 4000–200 cm^{-1} range using a KBr disc on a Perkin–Elmer 783 spectrophotometer. The magnetic susceptibility values were calculated using the equation $\chi = 2.83 (\text{m.T})^{-1/2}$.

The diamagnetic adjustments were made using Pascal's constant, and the calibrant was $\text{Hg}[\text{Co}(\text{SCN})_4]$. On a Varian E112 X-band spectrometer, the copper complexes' ESR spectra were obtained at 300 and 77 K.

2.1 Preparation of ligands 2 (a-i)

In 50 mL of dimethylformamide (DMF), 2(phenylselanyl)benzenamine was mixed with 12 mmol of sodium borohydride and stirred continuously at 0–5°C. After dilution with an equal volume of DMF, 10 mmol of phenylquinoline compounds 1(a-i) were added drop wise to the resulting solution. Reactions were completed in 60–90 minutes. The extractions were carried out in dichloromethane under vacuum. The organic layer was washed several times with brine solution before being dried over anhydrous sodium sulphate. The solvent was extracted using a rota evaporator, and the liquid was purified using a silica column and chloroform-methanol (8:2) as the eluant.

2a Yield: 74 %. Anal. calcd for $\text{C}_{27}\text{H}_{18}\text{Cl}_2\text{N}_2\text{Se}$: C, 62.33; H, 3.43; N, 5.38 DMSO- d_6 ; Found: C, 62.35; H, 3.41; N, 5.38. FAB mass spectrometry (FAB-MS) m/z 521[M+1]. ^1H NMR (400 MHz, CDCl_3 , δ , ppm): 6.32 (s, 1H), 6.40–7.12 (m, 4H), 7.18 (s, 1H), 7.16 (d, 1H), 7.14 (d, 1H), 7.22–7.42 (m, 4H), 7.42–7.48(d, 2H), 7.52–7.60 (m, 3H), 9.27 (s, -NH). ^{13}C NMR (400 MHz, DMSO- d_6): 138.9 (C-2), 102.1 (C-3), 164.6 (C-4), 130.1 (C-5), 118.8 (C-6), 131.8 (C-7), 116.3 (C-8), 148.1 (C-9), 117.7 (C-10), 133.4 (C-11), 129.2 (C-12), 126.9 (C-13), 134.9 (C-14), 130.3 (C-15). 132.6 (C-16), 153.1 (C-18), 122.3 (C-19), 130.2 (C-20), 127.2 (C-21), 132.8 (C-22), 122.1 (C-23), 130.0 (C-25), 131.5 (C-26), 128.7 (C-27, C-28, C-29), 131.6 (C-30).

2b Yield: 73 %. Anal. calcd for $\text{C}_{27}\text{H}_{18}\text{Cl}_2\text{N}_2\text{Se}$: C, 62.33; H, 3.49; N, 5.38; Found: C, 62.38; H, 3.47; N, 5.39. FAB mass spectrometry (FAB-MS) m/z 521[M+1]. ^1H NMR (400 MHz, CDCl_3 , δ , ppm): 6.24 (s, 1H), 6.30–6.53 (m, 4H), 7.18 (d, 2H), 7.14(t, 1H), 7.20–7.32 (m, 4H), 7.34–7.38 (d, 2H), 7.42–7.60 (m, 3H), 9.24 (s, -NH) ^{13}C NMR (400 MHz, DMSO- d_6): 138.8 (C-2), 102.1 (C-3), 164.6 (C-4), 130.1 (C-5), 118.8 (C-6), 131.8 (C-7), 116.3 (C-8), 148.1 (C-9), 117.7 (C-10), 133.4 (C-11), 129.2 (C-12), 126.9 (C-13), 134.9 (C-14), 130.3 (C-15). 132.6 (C-16), 153.1 (C-18), 122.3 (C-19), 130.2 (C-20), 127.2 (C-21), 132.8 (C-22), 122.1 (C-23), 130.0 (C-25), 131.5 (C-26), 128.7 (C-27, C-28, C-29), 131.6 (C-30).

2cYield: 74 %. Anal. calcd for $\text{C}_{27}\text{H}_{17}\text{Cl}_3\text{N}_2\text{Se}$: C, 58.46; H, 3.09; N, 5.05; Found: C, 58.48; H, 3.08; N, 5.04. FAB mass spectrometry (FAB-MS) m/z 555 [M+1]. ^1H NMR (400 MHz, CDCl_3 , δ , ppm): 6.12 (s, 1H), 6.34 (d, 1H), 6.42 (d, 1H), 6.54 (s, 1H), 7.12 (s, 1H), 7.18 (d, 1H), 7.20 (d, 1H), 7.22–7.36 (m, 4H), 7.43–7.50 (d, 2H), 7.52–7.62 (m, 3H), 9.22 (s, -NH). ^{13}C NMR (400 MHz, DMSO- d_6): 138.1 (C-2), 102.1 (C-3), 164.6 (C-4), 131.4 (C-5), 119.1 (C-6), 137.4 (C-7), 110.8 (C-8), 149.5 (C-9), 115.9(C-10), 133.4 (C-11), 129.2 (C-12), 126.9 (C-13), 134.9 (C-14), 130.3 (C-15). 132.6 (C-16), 153.1 (C-18), 122.3 (C-19), 130.2 (C-20), 127.2 (C-21), 132.8 (C-22), 122.1 (C-23), 130.0 (C-25), 131.5 (C-26), 128.7 (C-27, C-28, C-29), 131.6 (C-30).

2d Yield: 72 %. Anal. calcd for $\text{C}_{27}\text{H}_{17}\text{Cl}_3\text{N}_2\text{Se}$: C, 58.46; H, 3.09; N, 5.05; Found: C, 58.48; H, 3.08; N, 5.04. FAB mass spectrometry (FAB-MS) m/z 555 [M+1]. ^1H NMR (400 MHz, CDCl_3 , δ , ppm): 6.12 (s, 1H), 6.34 (d, 1H), 6.42 (d, 1H), 6.54 (s, 1H), 7.14 (d, 2H), 7.18(t, 1H), 7.20–7.30 (m, 4H), 7.32–7.38 (d, 2H), 7.42–7.58 (m, 3H), 9.22 (s, -NH) ^{13}C NMR (400 MHz, DMSO- d_6): 138.9 (C-2), 102.2 (C-3), 164.6 (C-4), 131.4 (C-5), 119.1 (C-6), 137.4 (C-7), 116.8

(C-8), 149.5 (C-9), 115.9 (C-10), 135.7 (C-11), 132.6 (C-12, C-16), 126.9 (C-13, C-15), 130.8 (C-14), 153.1 (C-18), 122.3 (C-19), 130.2 (C-20), 127.2 (C-21), 132.8 (C-22), 122.1 (C-23), 130.0 (C-25), 131.5 (C-26), 128.7 (C-27, C-28, C-29), 131.6 (C-30).

2e Yield: 72 %. Anal. calcd for $C_{27}H_{18}Cl_2N_2OSe$: C, 60.47; H, 3.38; N, 5.22; Found: C, 60.48; H, 3.35; N, 5.21. FAB mass spectrometry (FAB-MS) m/z 537 [M+1]. 1H NMR (400 MHz, $CDCl_3$, δ , ppm): 6.10 (s, 1H), 6.22 (d, 1H), 6.32 (d, 1H), 6.36 (s, 1H), 7.10 (s, 1H), 7.12 (d, 1H), 7.14 (d, 1H), 7.18-7.32 (m, 4H), 7.34-7.42 (d, 2H), 7.52-7.62 (m, 3H), 9.18 (s, -NH), 9.84 (s, -OH). ^{13}C NMR (400 MHz, DMSO- d_6): 138.1 (C-2), 102.1 (C-3), 164.6 (C-4), 131.4 (C-5), 119.1 (C-6), 161.6 (C-7), 110.8 (C-8), 149.5 (C-9), 115.9 (C-10), 133.4 (C-11), 129.2 (C-12), 126.9 (C-13), 134.9 (C-14), 130.3 (C-15), 132.6 (C-16), 153.1 (C-18), 122.3 (C-19), 130.2 (C-20), 127.2 (C-21), 132.8 (C-22), 122.1 (C-23), 130.0 (C-25), 131.5 (C-26), 128.7 (C-27, C-28, C-29), 131.6 (C-30).

2f Yield: 74 %. Anal. calcd for $C_{27}H_{18}Cl_2N_2OSe$: C, 60.47; H, 3.38; N, 5.22; Found: C, 60.48; H, 3.33; N, 5.21. FAB mass spectrometry (FAB-MS) m/z 537 [M+1]. 1H NMR (400 MHz, $CDCl_3$, δ , ppm): 6.11 (s, 1H), 6.24 (d, 1H), 6.32 (d, 1H), 6.44 (s, 1H), 7.11 (d, 2H), 7.16 (t, 1H), 7.18-7.30 (m, 4H), 7.30-7.38 (d, 2H), 7.38-7.54 (m, 3H), 9.18 (s, -NH), 10.11 (1H, s, OH). ^{13}C NMR (400 MHz, DMSO- d_6): 138.9 (C-2), 102.2 (C-3), 164.6 (C-4), 131.4 (C-5), 106.1 (C-6), 161.6 (C-7), 102.1 (C-8), 149.5 (C-9), 110.4 (C-10), 135.7 (C-11), 132.6 (C-12, C-16), 126.9 (C-13, C-15), 130.8 (C-14), 153.1 (C-18), 122.3 (C-19), 130.2 (C-20), 127.2 (C-21), 132.8 (C-22), 122.1 (C-23), 130.0 (C-25), 131.5 (C-26), 128.7 (C-27, C-28, C-29), 131.6 (C-30).

2g Yield: 71 %. Anal. calcd for $C_{27}H_{19}ClN_2Se$: C, 66.74; H, 3.94; N, 5.77; Found: C, 66.78; H,

3.93; N, 5.75. FAB mass spectrometry (FAB-MS) m/z 487 [M+1]. 1H NMR (400 MHz, $CDCl_3$, δ , ppm): 6.12 (s, 1H), 6.34 (d, 1H), 6.42 (d, 1H), 6.54 (s, 1H), 6.94-7.34 (m, 5H), 7.42-7.46 (d, 2H), 7.52-7.62 (m, 3H), 9.22 (s, -NH). ^{13}C NMR (400 MHz, DMSO- d_6): 138.1 (C-2), 102.1 (C-3), 164.6 (C-4), 131.4 (C-5), 119.1 (C-6), 137.4 (C-7), 110.8 (C-8), 149.5 (C-9), 115.9 (C-10), 138.2 (C-11), 126.3 (C-12, C-16), 128.6 (C-13, C-15), 128.0 (C-14), 153.1 (C-18), 122.3 (C-19), 130.2 (C-20), 127.2 (C-21), 132.8 (C-22), 122.1 (C-23), 130.0 (C-25), 131.5 (C-26), 128.7 (C-27, C-28, C-29), 131.6 (C-30).

2h Yield: 74 %. Anal. calcd for $C_{27}H_{20}N_2OSe$: C, 69.38; H, 4.31; N, 5.99; Found: C, 69.39; H, 4.35; N, 5.95. FAB mass spectrometry (FAB-MS) m/z 469 [M+1]. 1H NMR (400 MHz, $CDCl_3$, δ , ppm): 6.10 (s, 1H), 6.25 (d, 1H), 6.40 (d, 1H), 6.52 (s, 1H), 6.94-7.34 (m, 5H), 7.42-7.46 (d, 2H), 7.50-7.60 (m, 3H), 9.22 (s, -NH), 10.12 (s, 1H). ^{13}C NMR (400 MHz, DMSO- d_6): 138.1 (C-2), 102.1 (C-3), 164.6 (C-4), 131.4 (C-5), 106.1 (C-6), 161.6 (C-7), 101.2 (C-8), 149.5 (C-9), 115.9 (C-10), 134.2 (C-11), 126.3 (C-12, C-16), 128.6 (C-13, C-15), 128.1 (C-14), 122.3 (C-19), 130.2 (C-20), 127.2 (C-21), 132.8 (C-22), 122.1 (C-23), 130.0 (C-25), 131.5 (C-26), 128.7 (C-27, C-28, C-29), 131.6 (C-30).

2i Yield: 74 %. Anal. calcd for $C_{27}H_{20}N_2Se$: C, 71.23; H, 4.37; N, 6.39; Found: C, 71.25; H, 4.35; N, 6.37. FAB mass spectrometry (FAB-MS) m/z 451 [M+1]. 1H NMR (400 MHz, $CDCl_3$, δ , ppm): 6.32 (s, 1H), 6.52-7.22 (m, 4H), 6.94-7.34 (m, 5H), 7.42-7.46 (d, 2H), 7.52-7.62 (m, 3H), 9.22 (s, -NH). ^{13}C NMR (400 MHz, DMSO- d_6): 138.9 (C-2), 102.1 (C-3), 164.6 (C-4), 130.0 (C-5), 118.8 (C-6), 131.8 (C-7), 116.3 (C-8), 148.1 (C-9), 117.7 (C-10), 134.2 (C-11), 126.3 (C-12, C-16), 128.6 (C-13, C-15), 128.1 (C-14), 122.3 (C-19), 130.2 (C-20), 127.2 (C-21), 132.8 (C-22), 122.1 (C-23), 130.0 (C-25), 131.5 (C-26), 128.7 (C-27, C-28, C-29), 131.6

(C-30).

2.2 Preparation of metal chelates [3a-i (CuL¹(OAc)₂-CuL⁹(OAc)₂)]

Equimolar hot ethanolic solutions of phenylselanylquinoline derivative and copper acetate (0.05 M) were placed in a round bottom flask at room temperature; the reacting mixture was stirred and allowed to precipitate. The solid product was then separated with methanol and hexane and washed repeatedly. The remaining metal complexes were prepared with the same procedure. The metal chelates were dried in a vacuum desiccators over fused calcium chloride.

3a (CuL¹(OAc)₂): Yield: 68%. Anal. calcd for C₃₁H₂₄Cl₂CuN₂O₄Se: C 53.04, H 3.43; N 3.99; Found: C 53.06; H 3.46; N 3.96. FTIR (KBr): 3186 v(N-H), 1170 v(C-N), 1632 v(C=N), 550 v(Cu-N). FAB mass: 701 m/z [M+1]. μ_{eff} (BM) = 1.86; Δ_m (mho cm² mol⁻¹) = 20.

3b (CuL²(OAc)₂): Yield: 69%. Anal. calcd for C₃₁H₂₄Cl₂CuN₂O₄Se: C 53.04; H 3.43; N, 3.99; Cu, 9.05. Found: C, 53.06, H, 3.46; N 3.96. Cu 9.04. FTIR (KBr): 1632 v(C=N), 550 v(Cu-N). FAB mass: 701 m/z [M+1]. μ_{eff} (BM) = 1.88; Δ_m (mho cm² mol⁻¹) = 16.

3c (CuL³(OAc)₂): Yield: 67%. Anal. calcd for C₃₁H₂₃Cl₃CuN₂O₄Se: C 50.56, H 3.15, N 3.80, Found: C 50.53, H 3.12, N 3.78. FTIR (KBr): 1632 v(C=N), 550 v(Cu-N). FAB mass: 735 m/z [M+1]. μ_{eff} (BM) = 1.86; Δ_m (mho cm² mol⁻¹) = 20.

3d (CuL⁴(OAc)₂): Yield: 68%. Anal. calcd for C₃₁H₂₃Cl₃CuN₂O₄Se: C 50.56, H 3.15, N 3.80; Found: C 50.53, H 3.12, N 3.78. FTIR (KBr): 1632 v(C=N), 550 v(Cu-N). FAB mass: 735 m/z [M+1]. μ_{eff} (BM) = 1.96; Δ_m (mho cm² mol⁻¹) = 18.

3e (CuL⁵(OAc)₂): Yield: 68%. Anal. calcd for C₃₁H₂₄Cl₂CuN₂O₅Se: C 51.86, H 3.37, N 3.90,

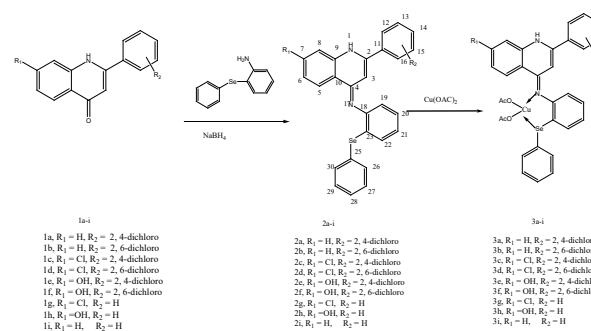
Found: C 51.84, H 3.34, N 3.88. FTIR (KBr): 3310 v(O-H), 1632 v(C=N), 550 v(Cu-N). FAB mass: 717 m/z [M+1]. μ_{eff} (BM) = 1.86; Δ_m (mho cm² mol⁻¹) = 18.

3f (CuL⁶(OAc)₂): Yield: 66%. Anal. calcd for C₃₁H₂₄Cl₂CuN₂O₅Se: C 51.86, H 3.37, N 3.90, Found: C 51.84, H 3.34, N 3.88. FTIR (KBr): 3310 v(O-H), 1632 v(C=N), 550 v(Cu-N). FAB mass: 717 m/z [M+1]. μ_{eff} (BM) = 1.86; Δ_m (mho cm² mol⁻¹) = 20.

3g (CuL⁷(OAc)₂): Yield: 68%. Anal. calcd for C₃₁H₂₅ClCuN₂O₄Se: C 55.78, H 3.78, N 4.20, Found: C 55.76, H 3.76, N 4.18. FTIR (KBr): 1632 v(C=N), 550 v(Cu-N). FAB mass: 667 m/z [M+1]. μ_{eff} (BM) = 2.06; Δ_m (mho cm² mol⁻¹) = 18.

3h (CuL⁸(OAc)₂): Yield: 67%. Anal. calcd for C₃₁H₂₆CuN₂O₅Se: C 57.37, H 4.04, N 4.32; Found: C 57.34, H 4.01, N 4.29. FTIR (KBr): 3310 v(O-H), 1632 v(C=N), 550 v(Cu-N). FAB mass: 649 m/z [M+1]. μ_{eff} (BM) = 1.86; Δ_m (mho cm² mol⁻¹) = 20.

3i (CuL⁹(OAc)₂): Yield: 69%. Anal. calcd for C₃₁H₂₆CuN₂O₄Se: C 58.82, H 4.14, N 4.43; Found: C 58.79, H 4.11, N 4.42. FTIR (KBr): 1632 v(C=N), 550 v(Cu-N). FAB mass: 633 m/z [M+1]. μ_{eff} (BM) = 1.96; Δ_m (mho cm² mol⁻¹) = 20. **Scheme**



3.0 Results and discussion

All copper complexes are stable at room

temperature, insoluble in water but soluble in dimethylsulfoxide (DMSO) and Methylcyanide. On the isolated solid complexes of Cu (II) ion with the ligands, elemental analyses (C, H, and N), IR, magnetic moments, molar conductance, ^1H NMR, and ESR were performed to understand the molecular structures of copper complexes. Analytical data from the ligands and their complexes were used to develop the empirical formula for the ligands and their complexes. Thin layer chromatography was used to compare the synthesized ligands to the starting materials. All complexes generated excellent elemental analysis results within the limits of experimental error (as shown in the Experimental section). All compounds disintegrated above 250°C , indicating their thermal stability.

IR spectra

The IR spectra of the ligands show a ν (C=N) peak in the $1654\text{--}1632\text{ cm}^{-1}$ range. All complexes have ν (C=N) bands at $1639\text{--}1580\text{ cm}^{-1}$ in their IR spectra [17], which are relocated to lower energy areas in the complexes compared to the free ligands. The change in the energy side of this band is most likely owing to an increase in the C=N bond order caused by the coordination of nitrogen with the copper atom. Complex spectra, exhibit two distinct bands attributable to $\nu_{\text{asy}}(\text{COO}^-)$ and $\nu_{\text{sy}}(\text{COO}^-)$ at $1630\text{--}1600$ and $1404\text{--}1340\text{ cm}^{-1}$, respectively.

This indicates that the complexes contain the carboxylate oxygen atom. The degree of separation between the $\nu_{\text{asy}}(\text{COO}^-)$ and $\nu_{\text{sy}}(\text{COO}^-)$ has also been utilised to determine the carboxylate group coordination mode. In copper complexes, the separation value between $\nu_{\text{asy}}(\text{COO}^-)$ and $\nu_{\text{sy}}(\text{COO}^-)$ was larger than 200 cm^{-1} , indicating that the carboxylate group in copper complexes of the ligands is coordinated monodentately [18]. Furthermore, the formation of complexes were also ascertained by the

presence of medium intensity bands at $576\text{--}578\text{ cm}^{-1}$ and $468\text{--}470\text{ cm}^{-1}$, which were assigned to ν (M-O) and ν (M-N), respectively [19]. Table 1 shows the characteristic peaks of ligands and complexes.

Table 1: IR characteristic peaks of synthesized ligands and complexes

Ligand / complex	ν C=N (cm $^{-1}$)	ν Cu-N (cm $^{-1}$)	ν (COO $^-$) _{asy} (cm $^{-1}$)	ν (COO $^-$) _{sy} (cm $^{-1}$)
2a	1635	-	-	-
2b	1630	-	-	-
2c	1622	-	-	-
2d	1629	-	-	-
2e	1610	-	-	-
2f	1635	-	-	-
2g	1625	-	-	-
2h	1612	-	-	-
2i	1622	-	-	-
3a	1625	520 – 550	1615	1380
3b	1620	530 – 550	1610	1370
3c	1610	520 – 550	1600	1390
3d	1620	530 – 550	1610	1370
3e	1620	520 – 550	1610	1380
3f	1625	520 – 550	1615	1350
3g	1615	530 – 550	1600	1380
3h	1610	520 – 550	1600	1370
3i	1590	530 – 550	1610	1400

Mass spectra

The structure of a substance can also be determined by mass spectra. The mass spectra of the ligand (2c) and its copper complex $[\text{CuL}^3(\text{OAc})_2]$ were recorded and their stoichiometric compositions were compared, as shown in Figures 1 & 2. The ion's stability and abundance are reflected in the intensity of these peaks [20]. The ligand (2c) has a molecular ion peak at 555 m/z , whereas its copper complex has a molecular ion peak at 735 m/z , indicating that the copper complexes have 1:1 stoichiometry.

Elemental analysis values resemble those estimated from molecular formulae assigned to these complexes, as evidenced by FAB-mass examinations of individual complexes. Similar mass spectral features were given to other ligands and their copper complexes.

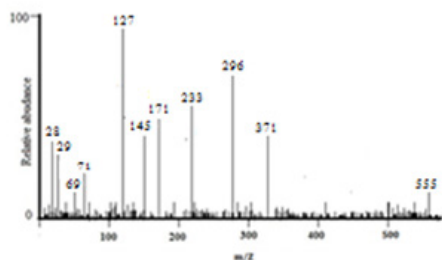


Fig. 1: Mass spectrum of ligand 2c

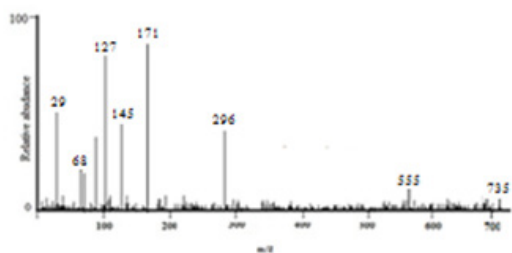


Fig. 2: Mass spectrum of copper complex 3c

¹H-NMR Spectra

The experimental part contains the ¹H and ¹³C-NMR spectra of ligands recorded in CDCl₃. Ligand 2c exhibits 6.12 (s, 1H), 6.34 (d, 1H), 6.42 (d, 1H), 6.54 (s, 1H), 7.12 (s, 1H), 7.18 (d, 1H), 7.20 (d, 1H), 7.22-7.36 (m, 4H), 7.43-7.50 (d, 2H), 7.52-7.62 (m, 3H), 9.22 (s, -NH). All of the protons were discovered to be in the expected location. The findings of this research add to the evidence for the bonding mode indicated in their IR spectra. The number of protons calculated from the integration curves and those calculated from the predicted CHN analysis values accord.

Electronic spectra

In DMSO as a solvent, the electronic spectra of the ligands and their copper complexes were recorded. The absorption spectra of the ligand show bands at 224 and 312 nm due to

$n-\pi^*$ and $\pi-\pi^*$ transitions within the Schiff base molecule. The electronic spectra of the analogous complex in DMSO reveal a band at 556 nm that may be given to the ${}^2B_{1g} \rightarrow {}^2A_{1g}$ transition [21, 22].

This band is suggestive of the square planar environment around the copper (II) ion and can be assigned to the ${}^2B_{1g} \rightarrow {}^2A_{1g}$ transition. Other complexes were given similar spectral characteristics. The benzenoid's $\pi-\pi^*$ transition / or $n-\pi^*$ (COO), the $>C=N$ - chromophore's $\pi-\pi^*$ transition, and the $>C=N$ - chromophore's $n-\pi^*$ transition, along with the secondary band of the benzene, display bands in the 200–225, 272–332 and 362–390 nm ranges in the electronic spectra of all the complexes.

There were also a few sharp lines in the spectra of the complexes in the 233–257 nm range that could be charge transfer bands. At ambient temperature, magnetic susceptibility experiments revealed that the copper complexes were paramagnetic. The magnetic moments of these complexes are extremely comparable to those of copper (II) complexes with no metal–metal interaction. At room temperature, the magnetic moment of the complex 3c is 1.86 BM, which is characteristic of mononuclear complexes of magnetically diluted d^9 systems with $S = 1/2$ spin state and square planar structure, with no metal–metal interaction along the axial position. Other copper complexes had comparable magnetic properties (Figure 3).

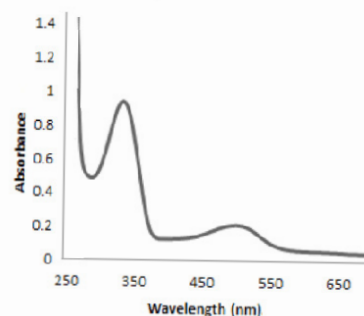


Fig. 3: UV spectrum of copper (II) complex 3c

ESR Spectra

Copper chelate ESR spectra (Figure 4) collected at 77 K in DMSO solution. It was found to have a g_{\parallel} value of 2.262, indicating that the metal-ligand link was a covalent. It was calculated that the planar distortion of copper (II) chelate due to regular geometrical arrangements ($f = g_{\parallel}/A_{\parallel}$) is 146.2. The results demonstrated that the biomolecular mechanism for biological reactions was facilitated by the distortion caused by regular square planar geometry around the copper centre [23, 24].

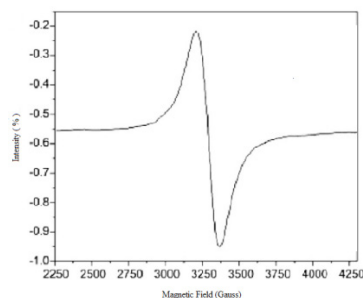


Fig. 4: ESR spectrum of copper complex 3c

Molar Conductance

For the 0.001 M solutions found in the experimental section, the molar conductance data for the copper complexes measured in DMSO solution. The complexes have values ranging from 10 to 29 $\text{mho cm}^2 \text{mol}^{-1}$, which is within the expected range of 1 to 35 $\text{mho cm}^2 \text{mol}^{-1}$ for non-electrolytes [25]. Because of the involvement of the acetate groups in coordination, the complexes are non-electrolytic. A chemical analysis of the CH_3COO^- ion that was not precipitated by the addition of FeCl_3 confirmed this.

3.1 TGA and DTA studies

The TGA and DTA curves of the Cu (II) complex (Figure 5) revealed that the complex is stable up to 250°C, with no weight loss before this temperature. At 250°C, the first

stage of deterioration began with the loss of three chlorine atoms, resulting in an 11.95 % functional weight loss. At 291°C, further degradation of the resultant complex resulted in the loss of the phenyl moiety, resulting in a functional weight loss of 11.40 %. At 340°C, the quinoline moiety was lost in the third stage of breakdown, resulting in a 47.95 % weight loss. Furthermore, the compound disintegrated up to 492°C due to the loss of the remaining organic moiety. Cupric oxide is the final weight of the residue.

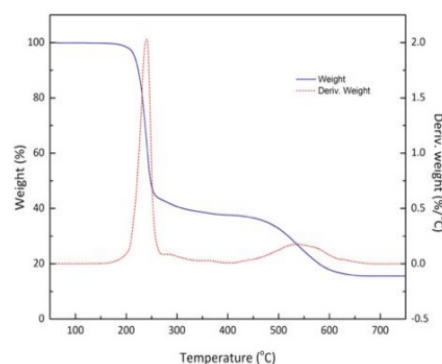


Fig. 5: TGA and DTA curves of Cu (II) complex 3c

3.2 Antimicrobial activities

In vitro antibacterial activity of the prepared ligands and their copper complexes were tested on bacterial and fungal species. One day before the experiment, bacterial and fungal cultures were inoculated in broth (inoculation medium) and incubated at 37 °C for overnight. To ensure uniform distribution, the inoculation medium containing 24 hours of produced crop was put to the nutrient medium and properly mixed. The solution was poured into Petri plates and allowed to set at room temperature, resulting in the production of gels. Wells (6 mm in diameter) were cut onto agar plates using sterile tubes. The wells were then filled to the agar surface with 0.1 mL of test chemicals dissolved in DMSO (200 μM / mL).

The plates were let to stand for an hour to aid in the diffusion of the medication solution. Following that, the plates were incubated at 37 °C for 24 hours for bacteria and 48 hours for fungus, and the diameter of the inhibitory zones was measured. Minimum inhibitory concentrations (MICs) were calculated using the serial dilution method. The MIC was determined to be the lowest concentration ($\mu\text{g} / \text{mL}$) of the drug that inhibits bacteria growth at 37 °C after 24 hours of incubation and fungal growth at 37 °C after 48 hours of incubation. The amount of dimethylsulfoxide in the medium had no effect on the growth of any of the bacteria examined.

Three Gram-negative bacteria: *Proteus vulgaris*, *Klebsiella pneumoniae*, and *Shigella flexneri*, three Gram-positive bacteria: *Staphylococcus aureus*, *Staphylococcus epidermidis*, and *Bacillus subtilis*, and three Fungi: *Aspergillus fumigatus*, *Aspergillus clavatus*, and *Candida albicans*, were tested in vitro for antibacterial and antifungal activity. Table 2 & 3 summarized the minimum inhibitory concentration (MIC) values of ligands and their copper complexes. A comparative analysis of ligands and their complexes (MIC values) shows that the antimicrobial activity of copper complexes is higher than that of free ligands

Heteroaromatic residues may be responsible for the antibacterial activity of the ligands. Antimicrobial activity is higher in compounds with a C=N group than in compounds with a C=C group. The enhanced activity of the complexes can also be described using Overtone's notion [26] and Tweedy's chelation theory [27]. The lipid membrane that surrounds the cell, according to Overtone's idea of cell permeability, enables only lipid-soluble molecules to pass through, making liposolubility a key element in limiting antimicrobial action. Liposolubility is an important factor in reducing antibacterial activity.

The polarity of the metal ion would be reduced to a greater degree during chelation due to the overlap of the ligand orbital and partial sharing of the positive charge of the metal ion with donor groups. It also increases the delocalization of π electrons around the entire chelate ring, which improves the lipophilicity of the complexes. Increased lipophilicity enhances complex penetration across lipid membranes and keeps metal binding sites in microorganism enzymes unblocked. These complexes also obstruct the cell's respiratory system, limiting the organism's capacity to develop by preventing protein synthesis.

As a result, microorganisms die. High solubility, particle fitness, metal ion size, and the presence of bulkier organic moieties all contribute to the complexes' higher antibacterial action. The development of a hydrogen connection between the active centre of cell components and the azomethine group disrupted normal cell function. The observed variance in copper complex activity across the diverse types of species tested could be explained by differences in cell wall and/or membrane structure. Copper complexes are likely to have increased lipophilicity due to the lipophilic group C=N and the large heteroaromatic ring system of quinoline, allowing them to penetrate the cell wall and facilitate unfavourable intracellular interactions.

Because it features a chlorine substitution at the 7th position, complex 3c demonstrated the best activity against *Aspergillus fumigatus* of all the complexes evaluated in this study. In comparison to other complexes, this electron withdrawing group boosts lipophilicity and increases activity. This shows that the molecular structure of the ligands and the type of complex generated affect antibacterial and antifungal action. The Cu (II) Schiff-base complex appears to have considerable antibacterial and antifungal activity, based on the preceding studies.

Table 2: Minimum inhibitory of concentration of the synthesized compounds against growth of bacteria (Microgram per milliliter)

Ligand / Complex	Gram +ve bacteria				Gram -ve bacteria	
	<i>B.subtilis</i>	<i>S.epidermidis</i>	<i>S.aureus</i>	<i>S.flexneri</i>	<i>K.pneumonia</i>	<i>P.vulgaris</i>
2a	19.4	23.7	18.5	25.9	19.6	20.4
2b	26.4	25.6	19.7	24.4	20.8	21.2
2c	17.6	18.1	17.4	19.4	18.8	18.4
2d	18.9	22.7	18.9	22.4	20.1	19.2
2e	21.5	21.7	21.6	23.6	22.4	23.2
3f	21.9	22.3	23.4	23.7	23.7	23.5
2g	22.4	23.4	24.2	24.7	22.8	23.4
2h	23.7	23.5	22.8	22.6	23.2	23.3
2i	23.2	23.7	22.4	23.5	22.7	22.8
3a	6.9	7.4	7.1	7.9	8.9	8.5
3b	7.8	8.6	9.1	10.7	9.6	10.2
3c	5.6	6.7	6.5	8.4	8.6	6.5
3d	5.9	6.4	6.1	6.9	7.9	6.4
3e	8.4	8.3	9.2	8.8	9.3	8.6
3f	8.7	8.8	8.9	9.1	8.7	9.2
3g	9.3	9.4	9.8	10.2	9.6	9.4
3h	10.4	10.5	10.4	10.1	9.8	10.6
3i	9.4	9.5	9.8	9.7	9.7	10.1
Ampicilin	1.9	1.8	1.7			
Gentamycin				1.8	1.6	1.7

Table 3: Minimum inhibitory of concentration of the synthesized compounds against growth of fungi (Microgram per millimeter)

Ligand \ Complex	Fungi		
	<i>C.albicans</i>	<i>A.fumigatus</i>	<i>A.clavatus</i>
2a	20.4	20.7	21.4
2b	20.9	21.3	21.7
2c	19.4	19.9	19.6
2d	19.6	20.9	20.6
2e	21.4	21.7	21.4
2f	22.4	23.7	24.8

2g	22.9	23.7	22.9
2h	23.7	24.4	23.6
2i	23.4	24.2	23.7
3a	7.9	7.4	8.3
3b	8.7	8.1	8.8
3c	6.9	6.2	7.1
3d	7.7	7.4	7.9
3e	9.3	8.6	9.7
3f	9.9	9.4	11.7
3g	10.6	11.6	10.4
3h	11.4	10.4	11.2
3i	11.3	10.2	11.2
Amphotericin	2.3	2.8	2.4

3.3 Cell lines and cell culture

Cells were grown in RPMI 1640 media supplemented with 10% (v/v) heat-inactivated fetal bovine serum (FBS), 100 units / mL penicillin, and 100 g / mL streptomycin. Both cell lines were grown in culture at 37°C in a 5 percent CO₂ environment.

3.3.1 MTT cytotoxicity assay

The cytotoxicity against HL-60 and MCF-7 cell line was determined using the 3-[4, 5-dimethyl-2-thiazolyl]-2, 5-diphenyl-2H-tetrazolium bromide (MTT) test. This assay is based on MTT reduction by mitochondrial dehydrogenases in living cells. Cells were inserted in a 96-well sterile microplate (5 - 104 cells / well) and cultured for 48 hours at 37°C in serum-free medium containing DMSO and a series of various concentrations (12.5, 25, 50, and 100 mM) of each drug or doxorubicin prior to the MTT test (positive control). After incubation, the medium was withdrawn and 40 mL of MTT (2.5 mg/mL) was added to each well. The incubation time was extended for an additional four hours. The purple formazan dye crystals were dissolved in 200 mL of dimethyl sulfoxide. The absorbance at 570 nm [28-30] was measured using a Spectra Max Paradigm

Multi-Mode microplate reader. To calculate relative cell viability, the mean proportions of viable cells compared to control cells were employed. The synthesized complexes were evaluated in vitro for activity against HL-60 and MCF-7 cell line using the MTT assay. The percentage of undamaged cells were calculated and compared to the control.

The activity of these complexes against the two cell lines was compared to that of doxorubicin.. All the complexes inhibited both cells in a dose-dependent manner. Ip [31] published comparative tests between comparable selenium and sulphur compounds, demonstrating that selenium inhibits cancer cell development far more effectively than sulphur.

In addition, selenium may have a multi-modal mechanism for inhibiting cellular transformation. El-Bayoumi [32] eventually discovered evidence to support this hypothesis by expanding the studies to other comparable sulphur and selenium compounds. Synthesized complexes were investigated in this light.

3d, 3a, and 3b demonstrated moderate in vitro efficacy in terms of selectivity and as an orientative measure. At 100 mM, 3c was significantly active against two cell lines, HL-

60 and MCF-7 shown in Figure 6.

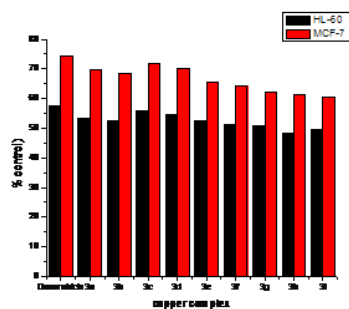


Fig. 6: Cytotoxicity against two cancer cell lines, according to the MTT assay at 100 μ M.

Table 4: IC_{50} value of the nine products against the two cancer cell lines according to the MTT assay.

Compound	% of inhibition	
	HL-60	MCF-7
Doxorubicin	57.71	74.33
3a	53.43	69.52
3b	52.45	68.28
3c	55.72	71.82
3d	54.64	70.28
3e	52.34	65.42
3f	51.28	64.28
3g	50.85	62.32
3h	48.28	61.28
3i	49.35	60.3

3.4 Anti-inflammatory efficiency

Due to ethical concerns, purchasing and using animals for pharmaceutical research is a more difficult process. In light of these considerations, the current study focused on protein denaturation approach [33] for in vitro anti-inflammatory efficiency of metal chelates using the egg albumin method.

These chemical compounds may prevent protein denaturation, enhancing the anti-inflammatory action. When compared to Diclofenac (IC_{50} 50 μ g/mL), the produced copper chelate (IC_{50} 40 μ g/mL) displayed stronger inhibitory activity

than other chelates (IC_{50} 78–90 μ g/mL) due to the presence of redox and chemical molecular moiety. The chelates' absorbance increased in comparison to the control, indicating that the protein was stabilising and thereby reducing the denaturation process. The biochemical interpretations revealed that the produced copper chelates were effective in reducing inflammation. Furthermore, clinical trials are required to determine the anti-inflammatory mechanism.

3.5 DNA binding studies

3.5.1 Absorption spectral studies

Electronic absorption spectroscopy was one of the most useful experimental techniques for studying metal ion-DNA interactions in metal complexes. Intercalation with DNA generally results in hypochromism and bathochromism due to the strong stacking interaction between aromatic chromophores and calf thymus-DNA (CT-DNA) base pairs. The absorption spectra demonstrate that the absorbance of complex 3c is clearly resolved at 289 nm. Increasing the concentration of CT-DNA resulted in hypochromic and bathochromic enhancements in its visible absorption spectra due to the formation of more stable complexes.

In the presence of increasing CT-DNA concentrations, complex 3c demonstrated a decrease in intensity, as well as a shift towards higher wavelengths hypochromicity (approximately 11 %) and bathochromic alterations (maximum: 21.1 nm) for its highest red-shift absorption peak (Figure 7) maxima. Using the change in absorbance values with increasing amounts of CT-DNA, the intrinsic binding constants (K_b) were calculated, and (K_b) was found to be $4.9 \times 10^5 \text{ M}^{-1}$, showing that complex 3c binds firmly to CT-DNA through intercalation [34, 35].

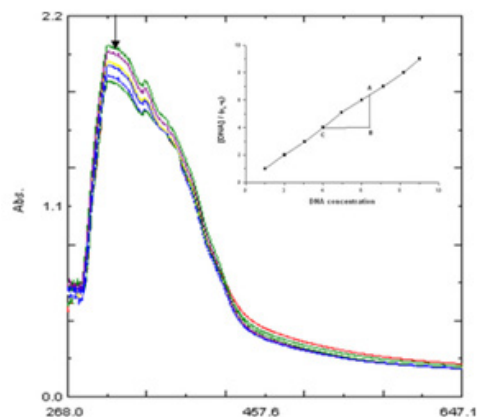


Fig. 7: Absorption spectral traces of copper complex 3c in Tris HCl buffer (0.01M, pH 7.2) upon addition of CT-DNA=0.5 μ m, =10 μ m, drug, 20 μ m; 30 μ m; 40 μ m; 50 μ m; Arrow shows the absorbance changing upon increase of DNA concentration.

3.5.2 Fluorescence studies

In Tris buffer, the complex 3c produces luminescence with a maximum at 450 nm at room temperature (pH 7.0-7.2). The intensity of the emission increases when CT DNA (Calf thymus DNA) is added to the complex, relative to the intensity of the complex alone (Figure 8). It has previously been observed that the addition of second molecules might attenuate this enhanced fluorescence, at least somewhat. Because the hydrophobic environment within the DNA helix restricts the accessibility of solvent water molecules to the duplex and thus restricts complex mobility at the binding site, the copper complex will interact strongly with CT-DNA via intercalation and will be effectively shielded by DNA.

This results in a reduction in vibrational modes of relaxation [36]. This increases the degree of amplification of the copper complex, which is consistent with the absorption spectra. Absorption spectra and viscosity measurements

supported the order of rise in complex emission rate.

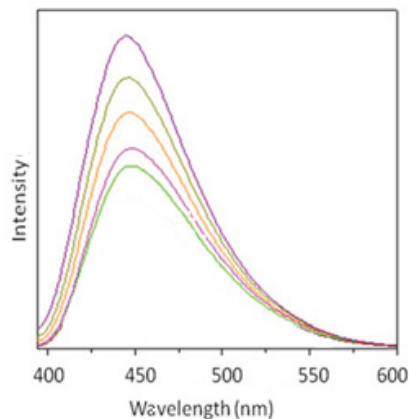


Fig. 8: Fluorescence emission of copper complex 3c in Tri-HCl buffer. Fluorescence intensity increasing CT-DNA concentrations (5 μ l, 10 μ l, 15 μ l, 20 μ l.....).

Inset:

Plots of relative emission intensity versus $[DNA]/[complex]$

3.5.3 Viscosity measurements

The viscosity data helped to explain the copper complex's binding modes with CT-DNA. In the absence of crystallographic structural data, the most essential tests of binding in solution are hydrodynamic assays sensitive to length change (for example, viscosity, sedimentation) [37]. A conventional intercalative mode causes a significant rise in the viscosity of DNA solution due to an increase in base pair separation at intercalation sites and hence an increase in total DNA length. Under the same conditions, a compound that binds primarily in the DNA grooves via partial and non-classical intercalation typically produces a negative or no shift in DNA solution viscosity.

By altering the concentration of the complex, viscosity measurements on CT-DNA were undertaken to better understand the current complex's binding mechanism.. The effects of

the complex on the viscosity of rod-like DNA were illustrated in Figure 9. The viscosity of DNA increases as the concentration of the complex 3c increases. As a result of the observations, the complex's presence has a demonstrable impact on CT-DNA relative viscosity.

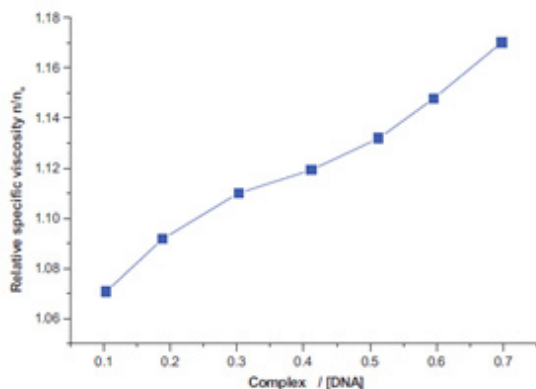


Fig. 9: Effects of increasing amount of copper Complex 3c on the relative viscosity of CT-DNA at $25 \pm 0.1^\circ\text{C}$

3.6 α -Glucosidase inhibition

The study on α -glucosidase inhibition for copper (II) complexes was described in Table 5, reflecting the IC_{50} values. The chelation of various metal acetate with inactive produced a perceptible increase in the inhibitory potential of ligand α -glucosidase and demonstrated the vital function of copper (II) centre during enzyme inhibition. This research predicts the concentration- dependent inhibition of α -glucosidase induced by the copper complexes (II) [38]. Among the complexes tested, the copper (II) complex 3c was highly potent α -glucosidase inhibitors ($\text{IC}_{50} = 0.20 \mu\text{M}$) and was approximately 200 times more active than the deoxynojirimycin (DNJ) ($\text{IC}_{50} = 300 \mu\text{M}$) standard α -glucosidase inhibitor. Copper (II) complex 3c was the most potent α -glucosidase inhibitor tested ($\text{IC}_{50} = 0.20 \mu\text{M}$) and was roughly 200 times more active than the DNJ ($\text{IC}_{50} =$

$300 \mu\text{M}$) standard α -glucosidase inhibitor. The active site residues of α -glucosidase (imidazole and carboxy groups) interact with metal (II) ions through soft electron donors like imidazole nitrogen, which inhibits the enzyme. The presence and position of substituents in the complex $[\text{Cu}^3(\text{OAc})_2]$ influence α -glucosidase inhibition. The inhibitory results indicate that the copper complex 3c can more easily occupy the active α -glucosidase sites than the conventional DNJ. As a result of its redox characteristics and molecular scaffolds, copper complex is an effective inhibitor of α -glucosidase.

Table 5: α -glucosidase inhibition activity of copper (II) complexes.

Complex/ Standard	IC_{50} (μM)
3a	0.55 ± 0.4
3b	0.86 ± 0.5
3c	0.20 ± 0.02
3d	0.55 ± 0.4
3e	0.99 ± 0.03
3f	0.84 ± 0.01
3g	1.10 ± 0.2
3h	1.11 ± 0.1
3i	1.12 ± 0.2
DNJ	DNJ 300 ± 0.5

3.7 Cholinesterase inhibitory activity

Cholinesterase inhibitors (ChEIs) are a class of drugs that increase cholinergic activity in the brain to improve memory, efficiency, and reduce psychiatric and behavioural disorders. Using a modified Ellman method [39], the AChE and BuChE inhibitory activities of the synthesized phenylselanylquinoline derivative were determined and compared to Galantamine and Rivastigmine as standards. Some acetylcholinesterase inhibitors (donepezil, galantamine, and rivastigmine) were used to treat AD symptoms.

Table 6 summarises the IC_{50} values for AChE and BuChE inhibitions. The heavily conjugated phenylselanylquinoline derivative, like ordinary

Galantamine ($IC_{50} = 2.41 \mu\text{M}$), showed the highest inhibition against AChE with an IC_{50} value of $0.20 \mu\text{M}$ and Rivastigmine ($IC_{50} = 3.03 \mu\text{M}$). The IC_{50} values obtained showed that phenylselanylquinoline derivatives, as opposed to Galantamine, serve as a selective inhibitor of AChE through a hydrophobic interaction and an interaction between π - π interactions. The fused aromatic nuclei with higher inhibitory AChE potencies are illuminated by the aromatic centre than their similar molecules with only one or two fused ring systems.

The best inhibitors for acting as powerful AChE inhibitors have fused aromatic properties. The azomethine moiety also promotes tight binding to the AChE active site, effectively inhibiting choline substrate hydrolysis.

As a result, the azomethine, quinoline, lipophilic moieties on conjugated aromatic centres, may be the primary prerequisite for anti-AChE activity. The inhibitory activities were attributed to the conjugated fused aromatic core moieties, according to the findings. Kinetic studies with AChE and BuChE, as well as ligand, were carried out to better understand the nature of their binding interactions. The ligand kinetic characteristics and inhibitory features were determined using the plot (Lineweaver-Burk reciprocal plot) representation.

With AChE and BuChE, the observed K_m and V_{max} values of ligand 2c at different concentrations are mentioned. As can be seen in Figure 10, increasing concentration changed both the slopes (lower V_m) and intercepts (higher K) (0.2, 0.4, 0.6 and 1.0 mM). This activity indicates that the ligand 2c inhibits AChE.

As shown in Figure 11, the ligand 2c inhibited BuChE and reduced the enzymatic velocity of catalytic BuChE-substrate reaction in a dose-dependent manner. The ligand could be bound to the catalytic active site and peripheral anionic

site when engaging with therapeutic targets, according to these experimental results.

Table 6: In vitro inhibition IC_{50} values (μM) and selectivity index of compound and Standards for AChE and BuChE.

compound	Inhibitory values IC_{50} (μM)		Selectivity index = IC_{50} (BuChE)/ IC_{50} (AChE)
	AChE	BuChE	
Ligand 2c	0.32 ± 0.15	3.2 ± 0.21	10
Galantamine	2.40 ± 0.10	17.30 ± 0.15	7.20
Rivastigmine	3.02 ± 0.20	0.30 ± 0.11	0.1

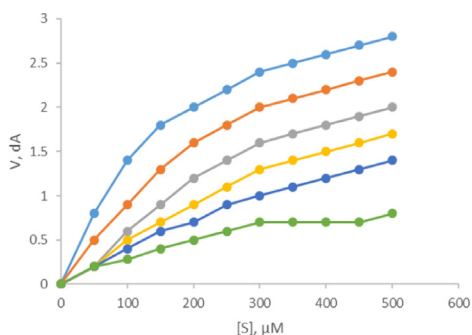


Fig. 10: Plot of AChE initial velocity with increasing substrate concentrations

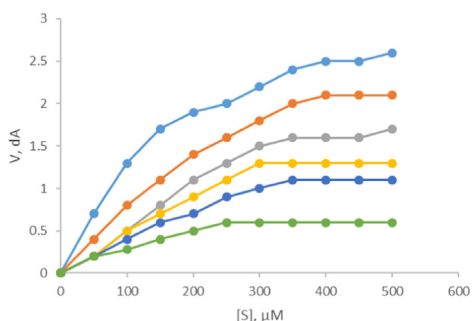


Fig. 11: Plot of BuChE initial velocity with increasing substrate concentration.

4.0 Conclusion

The synthesis, characterization, and biological evaluation of copper (II) complexes with organoselenium based schiff base ligands ((16E)-N-(2-phenylquinolin-4(1H)-ylidene)-2-(phenylselanyl)benzenamine) were investigated in this study. Spectroscopic examinations revealed that the copper complex connected with two carboxylate oxygen atoms and a copper atom via the quinoline moiety and organoselenium from the ligand. According to the analytical and spectral data, all copper complexes have a distorted square planar geometry with a metal to ligand ratio of 1:1.

Absorbance, fluorescence and viscosity measurements were used to evaluate the copper complexes' binding relationship with calf thymus DNA (CT-DNA). All of the complexes reacted with CT-DNA via an intercalation manner, according to these findings. According to the antimicrobial study, lipophilic and polar substituents like C=N and Se-N are likely to increase fungal and bacterial toxicity, and hence copper (II) complexes have a higher probability of interacting with nucleotide bases. Furthermore, it was discovered that complexing the ligand with the metal ion improves its anticancer activity in the MCF-7 cell line.

When compared to the standard inhibitor (DNJ), the synthesized Cu (II) complex showed effective inhibitory activity of α -glucosidase and could be used in the future for antidiabetic and other related disorders. They also contain Cholinesterase inhibitory action, which could be play a key role in the treatment of Alzheimer's disease in the future.

Acknowledgement

We thank the Head, Department of Chemistry, Manonmaniam Sundaranar University for providing the necessary facilities. This research did not receive any specific grant from funding agencies in the public, commercial, or not-for-

profit sectors.

Disclosure statement

No potential conflict of interest was reported by the authors.

5.0 References

1. Abdel-Rahman, L. H., Abu-Dief, A. M., Aboelez, M. O., & Abdel-Mawgoud, A. A. H. DNA interaction, antimicrobial, anticancer activities and molecular docking study of some new VO (II), Cr (III), Mn (II) and Ni (II) mononuclear chelates encompassing quaridentate imine ligand. *Journal of Photochemistry and Photobiology B: Biology*, 2017, 170, 271-285.
2. Abdel-Rahman, L. H., Abu-Dief, A. M., Shehata, M. R., Atlam, F. M., & Abdel-Mawgoud, A. A. H. Some new Ag (I), VO (II) and Pd (II) chelates incorporating tridentate imine ligand: Design, synthesis, structure elucidation, density functional theory calculations for DNA interaction, antimicrobial and anticancer activities and molecular docking studies. *Applied Organometallic Chemistry*, 2019, 33(4), 4699.
3. Abdel-Rahman, L. H., Abu-Dief, A. M., Adam, M. S. S., & Hamdan, S. K. Some new nano-sized mononuclear Cu (II) Schiff base complexes: design, characterization, molecular modeling and catalytic potentials in benzyl alcohol oxidation. *Catalysis Letters*, 2016, 146(8), 1373-1396.
4. Al-Saeedi, S. I., Abdel-Rahman, L. H., Abu-Dief, A. M., Abdel-Fatah, S. M., Alotaibi, T. M., Alsahme, A. M., & Nafady, A. Catalytic oxidation of benzyl alcohol using nanosized Cu/Ni schiff-base complexes and their metal oxide nanoparticles. *Catalysts*, 2018, 8(10), 452.
5. Adam, M. S. S., Abdel-Rahman, L. H., Abu-Dief, A. M., & Hashem, N. A. Synthesis, catalysis, antimicrobial activity, and DNA interactions of new Cu (II)-Schiff base complexes. *Inorganic and Nano-Metal Chemistry*, 2020, 50(3), 136-150.
6. Abdel-Rahman, L. H., Abu-Dief, A. M., & Abdel-Mawgoud Azza, A. H. Novel Di-and Tri-azomethine compounds as chemo sensors for the detection of various metal ions. *Int J Nano Chem*, 2019, 5, 1-17.
7. Fisher, A. Cholinergic modulation of amyloid precursor protein processing with emphasis on M1 muscarinic receptor: perspectives and challenges in treatment of Alzheimer's disease. *Journal of neurochemistry*, 2012, 120, 22-33.
8. Chan, K. Y., Wang, W., Wu, J. J., Liu, L., Theodoratou, E., Car, J & Global Health Epidemiology Reference Group (GHERG). Epidemiology of Alzheimer's disease and other forms of dementia in China, 1990–2010: a systematic

- review and analysis. *The Lancet*, 2013, 381(9882), 2016-2023.
9. Tiglani, D., Salahuddin, Mazumder, A., Yar, M. S., Kumar, R., & Ahsan, M. J. Benzimidazole-Quinoline Hybrid Scaffold as Promising Pharmacological Agents: A Review. *Polycyclic Aromatic Compounds*, 2021, 1-23.
 10. Pavlidis, N., Kofinas, A., Papanikolaou, M. G., Miras, H. N., Drouza, C., Kalampounias, A. G., & Leondaritis, G. Synthesis, characterization and pharmacological evaluation of quinoline derivatives and their complexes with copper (II) in in vitro cell models of Alzheimer's disease. *Journal of Inorganic Biochemistry*, 2021, 217, 111393.
 11. Golden, E. B., Cho, H. Y., Hofman, F. M., Louie, S. G., Schönthal, A. H., & Chen, T. C. Quinoline-based antimalarial drugs: a novel class of autophagy inhibitors. *Neurosurgical focus*, 2015, 38(3), E12.
 12. Wessjohann, L. A., Schneider, A., Abbas, M., & Brandt, W. Selenium in chemistry and biochemistry in comparison to sulfur, 2007, 997-1006.
 13. May, S. W., & Pollock, S. H. Selenium-based antihypertensives. *Drugs*, 1998, 56(6), 959-964.
 14. Muges, G., du Mont, W. W., & Sies, H. Chemistry of biologically important synthetic organoselenium compounds. *Chemical reviews*, 2001, 101(7), 2125-2180.
 15. De Oliveira C Brum, J., Neto, D. C. F., de Almeida, J. S. F., Lima, J. A., Kuca, K., França, T. C. C., & Figueroa-Villar, J. D. Synthesis of new quinoline-piperonal hybrids as potential drugs against Alzheimer's disease. *International journal of molecular sciences*, 2019, 20(16), 3944.
 16. Pinz, M. P., Dos Reis, A. S., Vogt, A. G., Krüger, R., Alves, D., Jesse, C. R & Luchese C. Current advances of pharmacological properties of 7-chloro-4-(phenylselanyl)quinoline: prevention of cognitive deficit and anxiety in Alzheimer's disease model. *Biomedicine & Pharmacotherapy*, 2018, 105, 1006-1014.
 17. Bansod, A. D., Mahale, R. G., & Aswar, A. S. Synthesis, characterization, electrical and biological studies on some bivalent metal complexes. *Russian Journal of Inorganic Chemistry*, 2007, 52(6), 879-883.
 18. Nakamoto, K. *Spectroscopy and Structure of Metal Chelate Compounds*, John Wiley: New York, 1988.
 19. Geary, W. J. The use of conductivity measurements in organic solvents for the characterization of coordination compounds. *Coordination Chemistry Reviews*, 1971, 7(1), 81-122.
 20. M Hamming, M, Foster, N, *Interpretation of Mass Spectra of Organic Compounds*, Academic Press: New York, wileyonlinelibrary.com/journal/aoc Copyright c_ 2011 John Wiley & Sons, Ltd, 1972.
 21. Chandra, S., & Gupta, L. K. EPR, mass, IR, electronic, and magnetic studies on copper (II) complexes of semicarbazones and thiosemicarbazones. *Spectrochimica Acta Part A: Molecular and Biomolecular Spectroscopy*, 2005, 61(1-2), 269-275.
 22. Lever, A. B. P., *Inorganic Electronic Spectroscopy*, 2nd edn. (Elsevier, New York) 1968.
 23. Singh, V. P. Synthesis, electronic and ESR spectral studies on copper (II) nitrate complexes with some acylhydrazines and hydrazones. *Spectrochimica Acta Part A: Molecular and Biomolecular Spectroscopy*, 2008, 71(1), 17-22.
 24. Kozlevčar, B. Structural analysis of a series of copper (II) coordination compounds and correlation with their magnetic properties. *Croatica Chemica Acta*, 2008, 81(2), 369-379.
 25. Geary, W. J. The use of conductivity measurements in organic solvents for the characterization of coordination compounds. *Coordination Chemistry Reviews*, 1971, 7(1), 81-122.
 26. Anjaneyulu, Y., & Rao, R. P. Preparation, characterization and antimicrobial activity studies on some ternary complexes of Cu (II) with acetylacetonone and various salicylic acids. *Synthesis and Reactivity in Inorganic and Metal-Organic Chemistry*, 1986, 16(2), 257-272.
 27. Dharmaraj, N., Viswanathamurthi, P., & Natarajan, K. Ruthenium (II) complexes containing bidentate Schiff bases and their antifungal activity. *Transition Metal Chemistry*, 2001, 26(1), 105-109.
 28. Hamdy, N. A., Anwar, M. M., Abu-Zied, K. M., & Awad, H. M. Synthesis, tumor inhibitory and antioxidant activity of new polyfunctionally 2-substituted 5, 6, 7, 8-tetrahydronaphthalene derivatives containing pyridine, thioxopyridine and pyrazolopyridine moieties. *Acta Pol Pharm Drug Res*, 2013, 70, 987-1001.
 29. Soliman, H. A., Yousif, M. N. M., Said, M. M., Hassan, N. A., Ali, M. M., Awad, H. M., & Abdel-Megeid, F. M. Synthesis of novel 1, 6-naphthyridines, pyrano [3, 2-c] pyridines and pyrido [4, 3-d] pyrimidines derived from 2, 2, 6, 6-tetramethylpiperidin-4-one for in vitro anticancer and antioxidant evaluation. *Der Pharma Chem*, 2014, 6, 394-410.
 30. Awad, H. M., Abd-Alla, H. I., Mahmoud, K. H., & El-Toumy, S. A. In vitro anti-nitrosative, antioxidant, and cytotoxicity activities of plant flavonoids: a comparative study. *Medicinal Chemistry Research*, 2014, 23(7), 3298-3307.
 31. Ip, C., & Ganther, H. E. Comparison of selenium and sulfur analogs in cancer prevention. *Carcinogenesis*, 1992, 13(7), 1167-1170.
 32. El-Bayoumy, K., Sinha, R., Pinto, J. T., & Rivlin, R. S. Cancer chemoprevention by garlic and garlic-containing sulfur and selenium compounds. *The Journal of nutrition*, 2006, 136(3), 864S-869S.
 33. Shunmugaperumal, T., & Kaur, V. In vitro anti-inflammatory and antimicrobial activities of azithromycin after loaded in chitosan-and tween 20-based oil-in-water macroemulsion for acne management. *Aaps Pharmscitech*, 2016, 17(3), 700-709.
 34. Prabhakara, M. C., Naik, H. B., Krishna, V., &

- Kumaraswamy, H. M. Binding and oxidative cleavage studies of DNA by mixed ligand Co (III) and Ni (II) complexes of quinolo [3, 2-b] benzodiazapine and 1, 10-phenanthroline. *Nucleosides, Nucleotides, and Nucleic Acids*, 2007, 26(5), 459-471.
35. Lamani, D. S., Reddy, K. V., Naik, H. B., Naik, H. P., & Naik, L. R. Synthesis, Characterization, and DNA Binding Studies of S₂N₂ Donor Bis-Mercaptoquinoline Co (II) and Ni (II) Metal Complexes: A New Class of Antimicrobial Agent. *Phosphorus, Sulfur, and Silicon*, 2010, 185(3), 550-558.
 36. Prakash Naik, H. R., Bhojya Naik, H. S., Ravikumar Naik, T. R., Naik, H. R., Lamani, D. S., & Aravinda, T. Pyrimido [4, 5-b] quinoline-2-thiol/ol: microwave-induced one-pot synthesis, DNA binding and cleavage studies. *Journal of Sulfur Chemistry*, 2008, 29(6), 583-592.
 37. Vaidyanathan, V. G., & Nair, B. U. Synthesis, characterization and binding studies of chromium (III) complex containing an intercalating ligand with DNA. *Journal of inorganic biochemistry*, 2003, 95(4), 334-342.
 38. Nikoogar, H., Mohammadi-Khanaposhtani, M., Imanparast, S., Faramarzi, M. A., Ranjbar, P. R., Mahdavi, M., & Larijani, B. Design, synthesis and in vitro α -glucosidase inhibition of novel dihydropyrano [3, 2-c] quinoline derivatives as potential anti-diabetic agents. *Bioorganic chemistry*, 2018, 77, 280-286.
 39. Pohanka, M., Hrabínová, M., Kuca, K., & Simonato, J. P. Assessment of acetylcholinesterase activity using indoxylacetate and comparison with the standard Ellman's method. *International journal of molecular sciences*, 2011, 12(4), 2631-2640.